Evaluation of the Unscanned Soft-Tissue Thermal Index

William D. O'Brien, Jr., *Fellow, IEEE*, and D. Scott Ellis

***Abstract*—The monopole-source solution was used to calculate the three-dimensional complex acoustic pressure field for focused circular apertures in a medium having homogeneous acoustic and thermal properties. The three source diameters were 1, 2, and 4 cm and the eight transmit f-numbers (ratio of the radius of curvature/source diameter) were 0.7, 1.0, 1.3, 1.6, 2.0, 3.0, 4.0, and 5.0. For these focused field geometries, eight ultrasonic frequencies were evaluated (1, 2, 3, 4, 5, 7, 9, and 12 MHz) from which the three-dimensional temperature distribution was calculated using the bio-heat transfer equation in homogeneous, perfused media (attenuation = absorption = 0.3 dB/cm-MHz; perfusion length: 1.0 cm). For each of the 192 cases, the acoustic field was normalized to the derated spatial peak, temporal average intensity ($I_{\mathrm{SPTA.3}}$) of 720 mW/cm^2, the maximum value allowed by the FDA 510(k) diagnostic ultrasound equipment approval process. Using the normalized acoustic field, the axial temperature increase profiles and the maximum temperature increases ($\Delta T_{\max}$) were determined for each case. Also, from the normalized acoustic field, the unscanned soft-tissue thermal index (TIS) was determined. In general, $\Delta T_{\max}$, TIS, and source power increase with increasing transmit f-number, source diameter, or frequency. The TIS generally underestimates (is less than) $\Delta T_{\max}$ for f-numbers ≤ 2, conditions for which $\Delta T_{\max} \leq 0.30$°C and TIS ≤ 0.40. This suggests that, for transmit f-numbers ≤ 2, TIS would not need to be displayed according to the ODS display requirements. With the exception of the longer-focus, larger-diameter, higher-frequency sources, TIS generally tracks $\Delta T_{\max}$ for f-numbers ≥ 3. These exceptions suggest a breakdown of the ODS procedures for calculating TIS.**

I. Introduction

When the U.S. Food and Drug Administration (FDA) initiated the regulation of diagnostic ultrasound equipment in the mid-1980s [1], [2], the FDA set application-specific intensity limits that could not be exceeded (Table I). These limits were not based on safety considerations. Rather, they were based on the output of diagnostic ultrasound systems that had been entered into interstate commerce prior to May 28, 1976, the date on which the Medical Devices Amendments were enacted. Diagnostic ultrasound manufacturers can still have their equipment approved using the application-specific limits process (Table I) for most indicated equipment uses. Alternately, manufacturers can have their equipment approved under the provisions of the *Standard for Real-Time Display of Thermal and Mechanical Indices on Diagnostic Ultrasound Equipment* (commonly called the Output Display Standard, ODS) [3]–[6]. Although the ODS does not specify upper limits, the FDA's implementation of the ODS stipulates regulatory upper limits to be 720 mW/cm^2 for the spatial peak, temporal average intensity, $I_{\mathrm{SPTA.3}}$, and 1.9 for the Mechanical Index for all but ophthalmologic applications [6]. The purpose of the ODS is to provide the capability for users of diagnostic ultrasound equipment to operate their systems at levels much higher than previously had been possible (see Table I) in order to have greater diagnostic capabilities. In doing so, the possibility was hypothesized for harm to the patient because of the potential for higher output levels. Therefore, the ODS requires that two biophysical indices be provided so that the equipment operator has displayed information available to make appropriate clinical decisions, *viz.*, benefit *vs.* risk, and to implement the ALARA (As Low As Reasonable Achievable) principle [7]. The two biophysical indices are the Thermal Index and the Mechanical Index. The Thermal Index provides information about tissue temperature increase, and the Mechanical Index provides information about the potential for cavitation. This contribution does not address the Mechanical Index.

The basic Thermal Index definition is [3]:

$$TI = \frac{W_0}{W_{\mathrm{DEG}}} \tag{1}$$

where W_0 is the source power of the diagnostic ultrasound system, and W_{DEG} is the source power required to increase the tissue temperature 1°C under very specific and conservative conditions. Three different Thermal Indices were developed to address three different tissue models and two different scan modes, that is, the soft-tissue thermal index (TIS), the bone thermal index TIB, and the cranial-bone thermal index TIC (Table II). The unscanned-mode typically is used clinically for spectral Doppler and M-Mode in which the ultrasound beam remains stationary for a period of time. Also, the unscanned-mode soft-tissue thermal index, as well as the TIB, are the only TI quantities that attempt to estimate temperature increase at locations other than at or near the source surface. The others estimate temperature increase at or near the source surface. This contribution is an evaluation only for the unscanned-mode soft-tissue thermal index.

Manuscript received December 7, 1998; accepted July 6, 1999. This work was supported in part by the NIH CA09067, NIH HD21687, and NIH HL58218.

W. D. O'Brien, Jr., is with the Bioacoustics Research Laboratory, Department of Electrical and Computer Engineering, University of Illinois, Urbana, IL 61801 (e-mail: wdo@uiuc.edu).

D. S. Ellis is with Andersen Consulting, Washington, DC 20006.

0885–3010/99$10.00 © 1999 IEEE

TABLE I
FDA PRE-AMENDMENTS LEVELS OF DIAGNOSTIC ULTRASOUND DEVICES [2]

Sites	Derated Intensity Values		
	I_{SPTA} (mW/cm^2)	I_{SPPA} (W/cm^2)	I_m (W/cm^2)
Cardiac	430	190	310
Peripheral vessel	720	190	310
Ophthalmic	17	28	50
Fetal imaging and other*	94	190	310

* Abdominal, intraoperative, small organ (breast, thyroid, testes), neonatal cephalic, adult cephalic.

TABLE II
OUTLINE OF THE THERMAL INDICES

	Scanned mode	Unscanned mode
Soft tissue	TIS at surface	TIS small aperture and large aperture
Bone at focus	TIS at surface	TIB
Bone at surface	TIC	TIC

II. Methodology and Definitions

The monopole-source solution for estimating tissue temperature increase of a focused ultrasound field was used [8]. The monopole-source solution does not restrict itself to a specific beam geometry, and thus has applicability to any arbitrarily shaped source aperture. Its solution consists of two steps. The first step determines the three-dimensional distribution of the complex acoustic pressure field $\mathbf{p}$ generated by an ultrasonic source from the solution to the lossy Helmholtz equation given by:

$$\nabla^2\mathbf{p} + \mathbf{k}^2\mathbf{p} = 0 \tag{2}$$

where $\mathbf{k}$ is the complex wave number $\mathbf{k} = k_0 - j\alpha$, and where k_0 and α are the wave number ($k_0 = \omega/c, \omega$ is the angular frequency, and c is the medium's propagation speed) and amplitude absorption coefficient, respectively. For a very small and spherically symmetric acoustic source (a monopole source) with angular frequency, ω, ω, in an unbounded fluid, the monopole-source solution of (2) is:

$$\mathbf{p} = \frac{G}{R}e^{-j\mathbf{k}R} = \frac{G}{R}e^{-\alpha R}e^{-jk_0R} \tag{3}$$

where the constant G is called the monopole-pressure amplitude and R is the outgoing radial distance (spherical coordinates for the monopole source). The acoustic pressure spatial distribution is determined by summing the individual fields at each field location from the N acoustic monopoles that conform to the source aperture geometry. The absorption coefficient α in (3) is replaced by the attenuation coefficient A because the loss of amplitude as the wave propagates is quantified by the attenuation coefficient.

The second step uses the computed three-dimensional acoustic pressure field to determine the temperature increase at any point in the medium. The bio-heat transfer equation is used to combine the processes of ultrasonic absorption, tissue perfusion, and heat conduction, that is,

$$\frac{\partial T}{\partial t} = \kappa\nabla^2 T - \frac{\Delta T}{\tau} + \frac{q_v}{c_v} \tag{4}$$

where T is the ambient temperature level, t is time, κ is the thermal diffusivity, ΔT is the temperature increase, τ is the perfusion time constant, c_v is the heat capacity per unit volume of the medium, $q_v = \frac{\alpha p_0^2}{\rho c}$ is the heat generated locally at a temporal-average rate per unit volume, $p_0^2 = \mathbf{p}\mathbf{p}^*$ is the squared magnitude of the complex acoustic pressure amplitude at a specific field location, and ρc is the medium's characteristic acoustic impedance (product of density, ρ, and propagation speed, c). A solution to (4) is used as the basis for the monopole-source solution to yield the temporal-dependent temperature increase at a distance r from a monopole (infinitesimal) heat source of volume dv, which is generating heat at a rate $q_v dv$ for a time t [9], that is,

$$\Delta T(t, r) = \frac{C}{r}\left\{e^{-r/L}\left[2 - \operatorname{erfc}\left(t^* - R^*\right)\right] + e^{r/L}\operatorname{erfc}\left(t^* + R^*\right)\right\} \tag{5}$$

where

$$C = \frac{q_v dv}{8\pi K} = \frac{\alpha p_0^2 dv}{8\pi \rho c K} \tag{5a}$$

$$K = c_v \kappa \tag{5b}$$

$$L = \sqrt{\kappa \tau} \tag{5c}$$

$$t^* = \sqrt{\frac{t}{\tau}} \tag{5d}$$

$$R^* = \frac{r}{\sqrt{4\kappa\tau}} = \frac{r}{2L} \tag{5e}$$

and where K is the thermal conductivity coefficient, L is the perfusion length, and erfc is the complementary error function. The steady-state solution of (5) is:

$$\Delta T(r) = \frac{2C}{r} e^{-rL}. \tag{6}$$

Using the point-source solution to the bio-heat transfer equation, (5) for the temporally dependent solution and (6) for the steady-state solution, the temperature increase at an observation point $P_{\text{obs}}(x_{\text{obs}}, y_{\text{obs}}, z_{\text{obs}})$ due to an infinitesimal heat source located at $P_{\text{hs}}(x_{\text{hs}}, y_{\text{hs}}, z_{\text{hs}})$ is given by [9]:

$$\Delta T(P_{\text{obs}}, P_{\text{hs}}) = \frac{2C}{s} e^{-s/L} \tag{7}$$

where s is the distance between $P_{\text{obs}}(x_{\text{obs}}, y_{\text{obs}}, z_{\text{obs}})$ and $P_{\text{hs}}(x_{\text{hs}}, y_{\text{hs}}, z_{\text{hs}})$. The temperature increase is calculated, using the superposition principle, by summing the infinitesimal heat source temperature increases, $\Delta T(P_{\text{obs}}, P_{\text{hs}})$, from every infinitesimal heat source location (P_{hs}) to the observation locations (P_{obs}). For this contribution, the temperature increase profile is calculated along the z-axis (z_{obs} locations).

The majority of axial temperature increases is reported for the steady-state solution. The maximum value of the axial steady-state temperature increase is denoted $\Delta T_{\max}$. In addition, the temporal dependency of axial temperature increase is reported and expressed in terms of time required for the temperature to reach 80% of its steady-state temperature increase, where the time and temperature at a specified axial location are denoted by $t_{80\%}$ and $\Delta T_{80\%}$, respectively.

For the unscanned soft-tissue thermal index, it was assumed that the tissue is homogeneous (in terms of both acoustic and thermal properties). The attenuation coefficient A (also referred to as a derating factor) and absorption coefficient α are both 0.3 dB/cm-MHz, density ρ is 1000 kg/m^3, propagation speed c is 1540 m/s, tissue perfusion L is 1 cm, and tissue thermal conductivity K is 0.006 W/cm^2. These are the values used in the ODS [3] and the values used herein.

The basis for the development of the unscanned TIS computations for the small and large aperture cases is discussed in detail elsewhere [3], [10], [11]. The two expressions for the TIS computations are based on the source aperture size. For a large aperture as shown in (8) (top

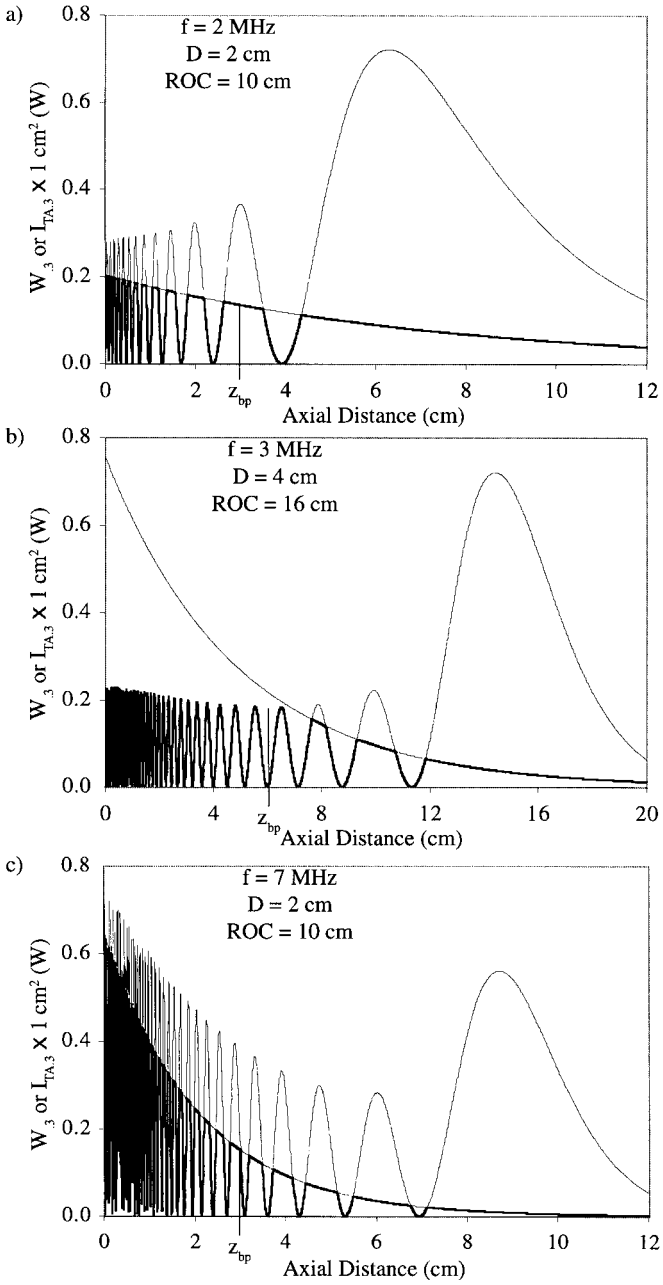

Fig. 1. Three examples of how the numerator of (8) is determined under the condition that the derated spatial-peak, temporal-average intensity $I_{\text{SPTA.3}}$ is 720 mW/cm^2. The derated acoustic power $W_{.3}(z)$ is the smooth exponentially decaying line, and the derated temporal-average intensity times an area of 1 cm^2 $I_{\text{TA.3}}(z) \times 1$ cm^2 is the oscillatory line. The bold line in these examples denotes the minimum of either $W_{.3}(z)$ or $I_{\text{TA.3}}(z) \times 1$ cm^2, that is, $\min\left\{W_{.3}(z); I_{\text{TA.3}}(z) \times 1 \text{ cm}^2\right\}$, as a function of axial distance. The solid vertical line for each example is the location of z_{bp}. (a) Frequency = 2 MHz, source diameter = 2 cm, ROC = 10 cm, $z_{\text{bp}} = 3.00$ cm, and $z_1 = 3.00$ cm, for which the maximum values of $I_{\text{TA.3}}(z) \times 1$ cm^2 are greater than $W_{.3}(z)$ in the region less than z_{bp}. (b) Frequency = 3 MHz, source diameter = 4 cm, ROC = 16 cm, $z_{\text{bp}} = 6.00$ cm, and $z_1 = 6.40$ cm, for which the maximum values $I_{\text{TA.3}}(z) \times 1$ cm^2 are less than $W_{.3}(z)$ in the region less than z_{bp}. (c) Frequency = 7 MHz, source diameter = 2 cm, ROC = 10 cm, $z_{\text{bp}} = 3.00$ cm, and $z_1 = 3.00$ cm, for which the maximum values of $I_{\text{TA.3}}(z) \times 1$ cm^2 are greater than $W_{.3}(z)$ in the region less than z_{bp} and for which the magnitude of $I_{\text{TA.3}}(z) \times 1$ cm^2 is greater near the transducer than in the focal region.

$$\mathrm{TIS} = \frac{\max\limits_{z_1 > z_{bp}} \left\{ \min \left\{ W_{.3}(z_1) ; I_{\mathrm{TA.3}}(z_1) \times 1\ \mathrm{cm}^2 \right\} \right\}}{\left(\frac{210}{f_c} \right)} \quad \text{for } A_{\mathrm{aprt}} > 1\ \mathrm{cm}^2 \tag{8}$$

of this page), where $W_{.3}(z_1)$ is the derated power at z_1, $I_{\mathrm{TA.3}}(z_1)$ is the derated temporal-average intensity at z_1, f_c is the ultrasound center frequency, A_{aprt} is the aperture (source) surface area, and z_1 is the axial distance greater than the axial break-point distance z_{bp}. The break-point distance was introduced into the TIS determination in order to avoid measurement inaccuracies introduced by attempting to measure intensities too close to the source surface, and for a circular source is 1.5 times the source diameter,

$$z_{\mathrm{bp}} = 1.5\sqrt{\frac{4}{\pi}A_{\mathrm{aprt}}} = 1.69\sqrt{A_{\mathrm{aprt}}}. \tag{9}$$

Three examples (Fig. 1) demonstrate how the numerator of (8) is determined, that is, where the maximum values of $I_{\mathrm{TA.3}}(z) \times 1\ \mathrm{cm}^2$ are greater than $W_{.3}(z)$ in the region less than z_{bp} [Fig. 1(a)], where the maximum values of $I_{\mathrm{TA.3}}(z) \times 1\ \mathrm{cm}^2$ are less than $W_{.3}(z)$ in the region less than z_{bp} [Fig. 1(b)] and where the maximum values of $I_{\mathrm{TA.3}}(z) \times 1\ \mathrm{cm}^2$ are greater than $W_{.3}(z)$ in the region less than z_{bp} and also where the magnitude of $I_{\mathrm{TA.3}}(z) \times 1\ \mathrm{cm}^2$ is greater near the skin surface than in the focal region [Fig. 1(c)]. The solid line in these three examples denotes the minimum of either $W_{.3}(z)$ or $I_{TA.3}(z) \times 1\ \mathrm{cm}^2$, that is, $\min\left\{W_{.3}(z) ; I_{\mathrm{TA.3}} \times 1\ \mathrm{cm}^2\right\}$, and z_1 is the location greater than z_{bp} (denoted by the short, solid vertical line) where the solid line is at its maximum value, that is, $\max\limits_{z_1 > z_{bp}} \left\{ \min \left\{ W_{.3}(z) ; I_{\mathrm{TA.3}} \times 1\ \mathrm{cm}^2 \right\} \right\}$. The basis for why $W_{.3}(z)$ or $I_{\mathrm{TA.3}}(z) \times 1\ \mathrm{cm}^2$ control maximum temperature increases for different situations can be found elsewhere [3], [10].

For a small aperture:

$$\mathrm{TIS} = \frac{W_0}{\left(\frac{210}{fc} \right)} \text{ for } A_{\mathrm{aprt}} \leq 1\ \mathrm{cm}^2. \tag{10}$$

All computations were made on either a SUN SparcStation 2, SUN SparcStation 20 or SUN UltraSparc 1. A monopole-source spacing on the transducer surface of $\lambda/4$ and a field spacing of 0.01 cm were used for the monopole-source solution. These were verified previously [8] to yield convergent asymptotic temperature increase values.

III. Results and Discussion

One hundred ninety-two cases have been investigated at eight frequencies (1, 2, 3, 4, 5, 7, 9, and 12 MHz), three source diameters D (1, 2, and 4 cm), and appropriate radii of curvature (ROC) to yield f-numbers (= ROC/D) of 0.7, 1.0, 1.3, 1.6, 2.0, 3.0, 4.0, and 5.0. This selection of frequencies, diameters, and transmit f-numbers was chosen to provide sufficient detail to evaluate TIS, $\Delta T_{\max}$, and other exposure trends over the diagnostic ultrasound frequency range.

All results reported herein are based on the derated spatial-peak, temporal-average intensity $I_{\mathrm{SPTA.3}}$ of 720 mW/cm^2. This value provides a common reference as well as a worst-case exposure condition based on the FDA limit for most diagnostic ultrasound equipment approved under the ODS procedures [6].

Fig. 2, 3, and 4 show, respectively, the maximum steady-state temperature increase $\Delta T_{\max}$; the unscanned soft-tissue thermal index TIS; and the source power W_0 as a function of f-number, source diameter D, and frequency. In general, $\Delta T_{\max}$, TIS, and W_0 increase as a function of increasing f-number, source diameter, or frequency. These trends follow the source power. As the f-number increases, and hence the ROC increases, the source power must increase in order to satisfy the 720 mW/cm^2 requirement because $I_{\mathrm{SPTA.3}}$'s distance from the source increases.

Direct comparison of the 192 $\Delta T_{\max}$-TIS pairs provides an understanding of how the maximum steady-state temperature increase $\Delta T_{\max}$ tracks its matched TIS value from the same computed acoustic pressure field. The paired $\Delta T_{\max}$ and TIS (Fig. 5) are grouped by f-number and shown as a function of frequency where the frequency axis is grouped by the three source diameters. A comparison of these 192 $\Delta T_{\max}$-TIS pairs against the TIS = $\Delta T_{\max}$ straight line is shown in Fig. 6(a). The minimum and maximum values of $\Delta T_{\max}$, TIS and $\frac{\Delta T_{\max}}{\mathrm{TIS}}$ are grouped by f-number and listed in Table III. At the lower f-numbers and at constant source diameters, both $\Delta T_{\max}$ and TIS decrease as a function of increasing frequency with $\Delta T_{\max}$ generally greater than TIS, that is, TIS underestimates $\Delta T_{\max}$ [Fig. 5(a–d)], and there is a general reversal of this trend for the higher f-numbers [Fig. 5(e–h)]. Both $\Delta T_{\max}$ and TIS tend to increase as a function of increasing f-number (Fig. 6a) where it is interesting to observe that the $\Delta T_{\max}$-TIS pairs roughly follow TIS = $\Delta T_{\max}$, suggesting that the TIS calculation reasonably estimates the computed $\Delta T_{\max}$. However, these cases need to be examined in greater detail as there are numerous $\frac{\Delta T_{\max}}{\mathrm{TIS}}$ values greater than 1 (Table III), that is, TIS underestimates $\Delta T_{\max}$ [under the straight line in Fig. (6)].

The four lowest f-number groups ($f/0.7$, $f/1.0$, $f/1.3$, $f/1.6$) include 96 $\Delta T_{\max}$-TIS pairs in which the maximum $\Delta T_{\max}$ value does not exceed 0.25°C (Table III) even though TIS generally underestimates (is less than) $\Delta T_{\max}$ [Fig. 5(a–d)]. The maximum $\frac{\Delta T_{\max}}{\mathrm{TIS}}$ value is 109 among these four f-number groups (Table III). The maximum

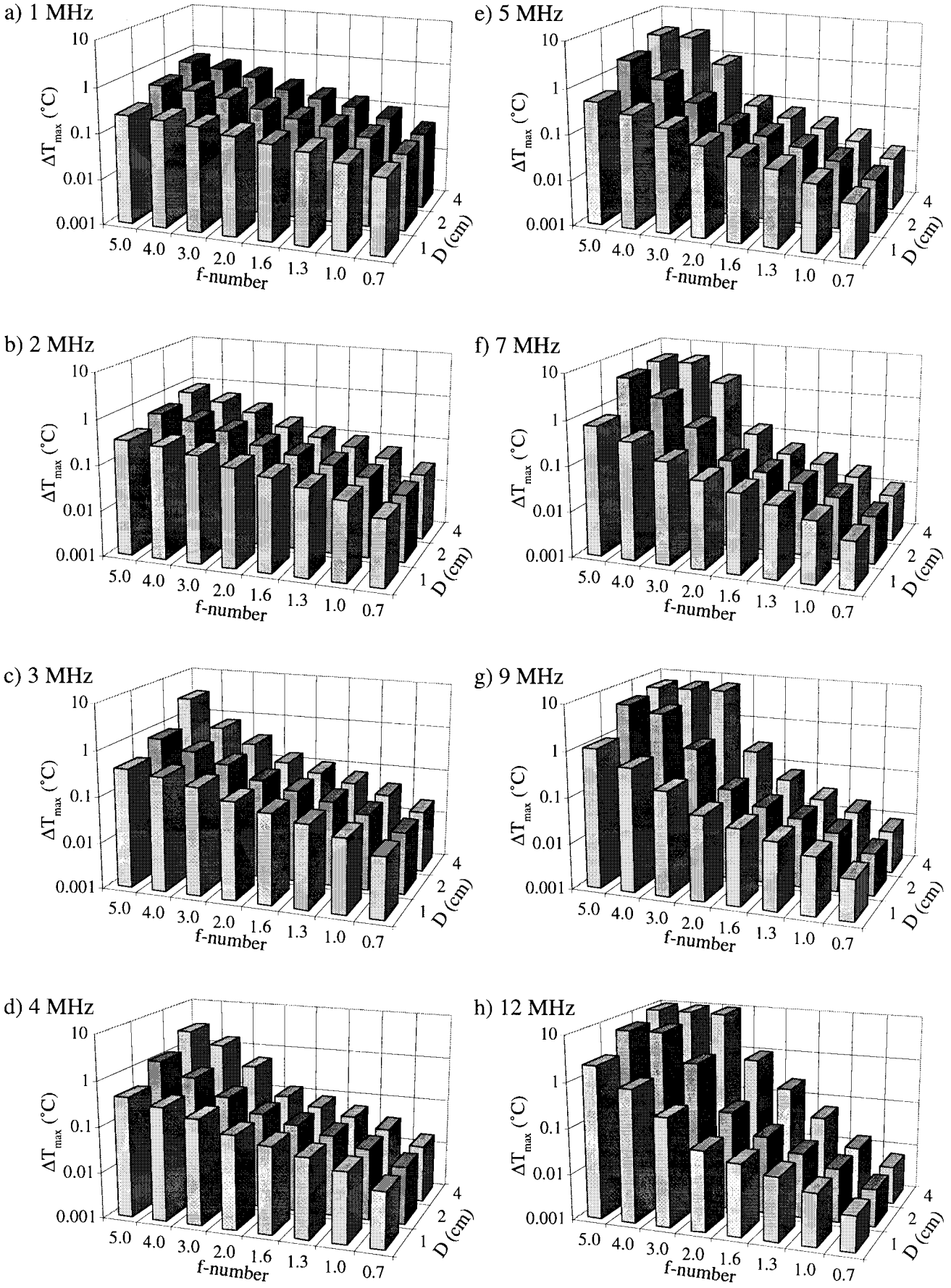

Fig. 2. Maximum steady-state temperature increase $\Delta T_{\max}$ as a function of f-number and source diameter D for each of the eight frequencies under the condition that the derated spatial-peak, temporal-average intensity $I_{\mathrm{SPTA.3}}$ is 720 mW/cm^2.

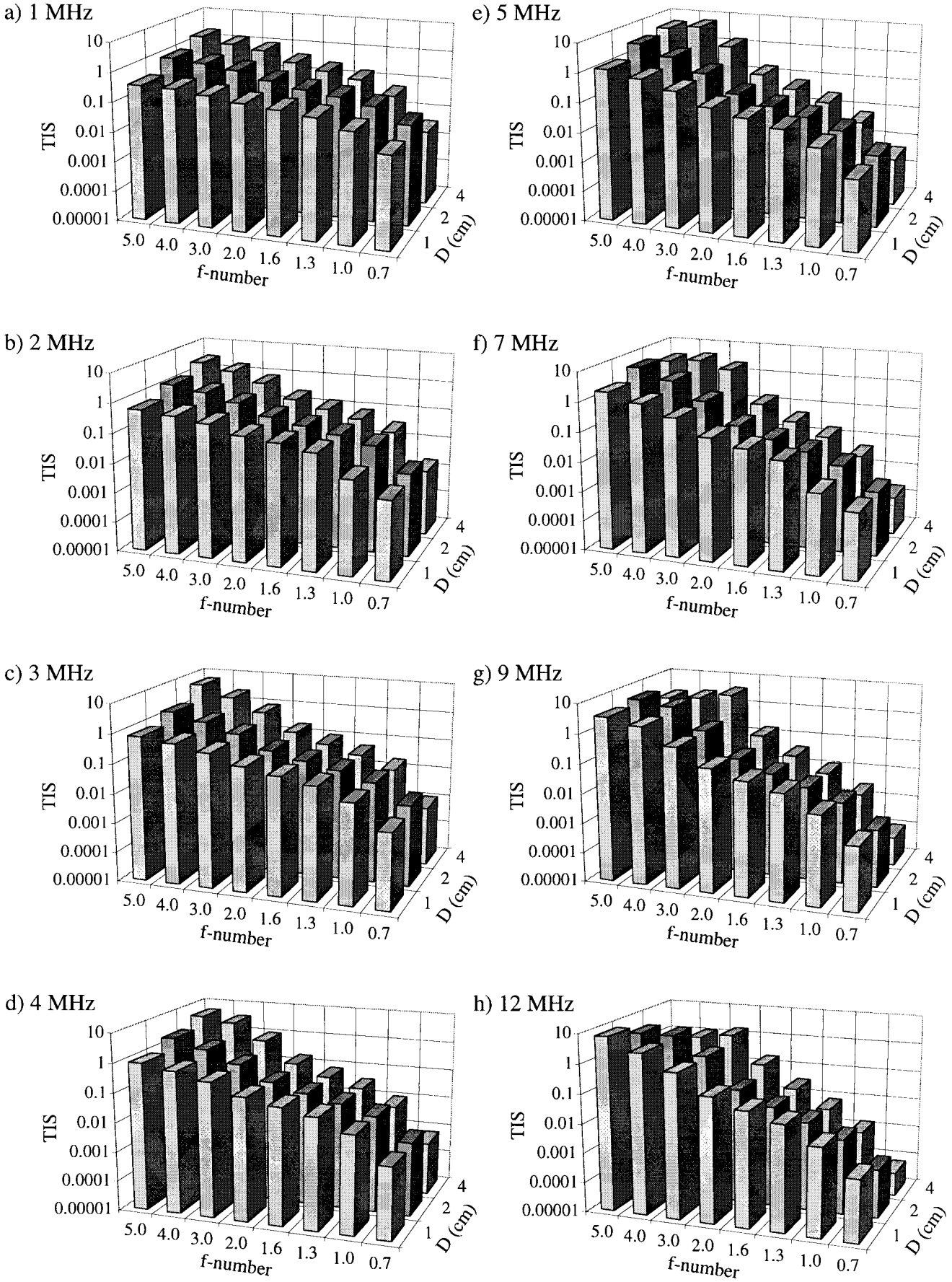

Fig. 3. Unscanned soft-tissue thermal index TIS as a function of f-number and source diameter D for each of the eight frequencies under the condition that the derated spatial-peak, temporal-average intensity $I_{\mathrm{SPTA.3}}$ is 720 mW/cm^2.

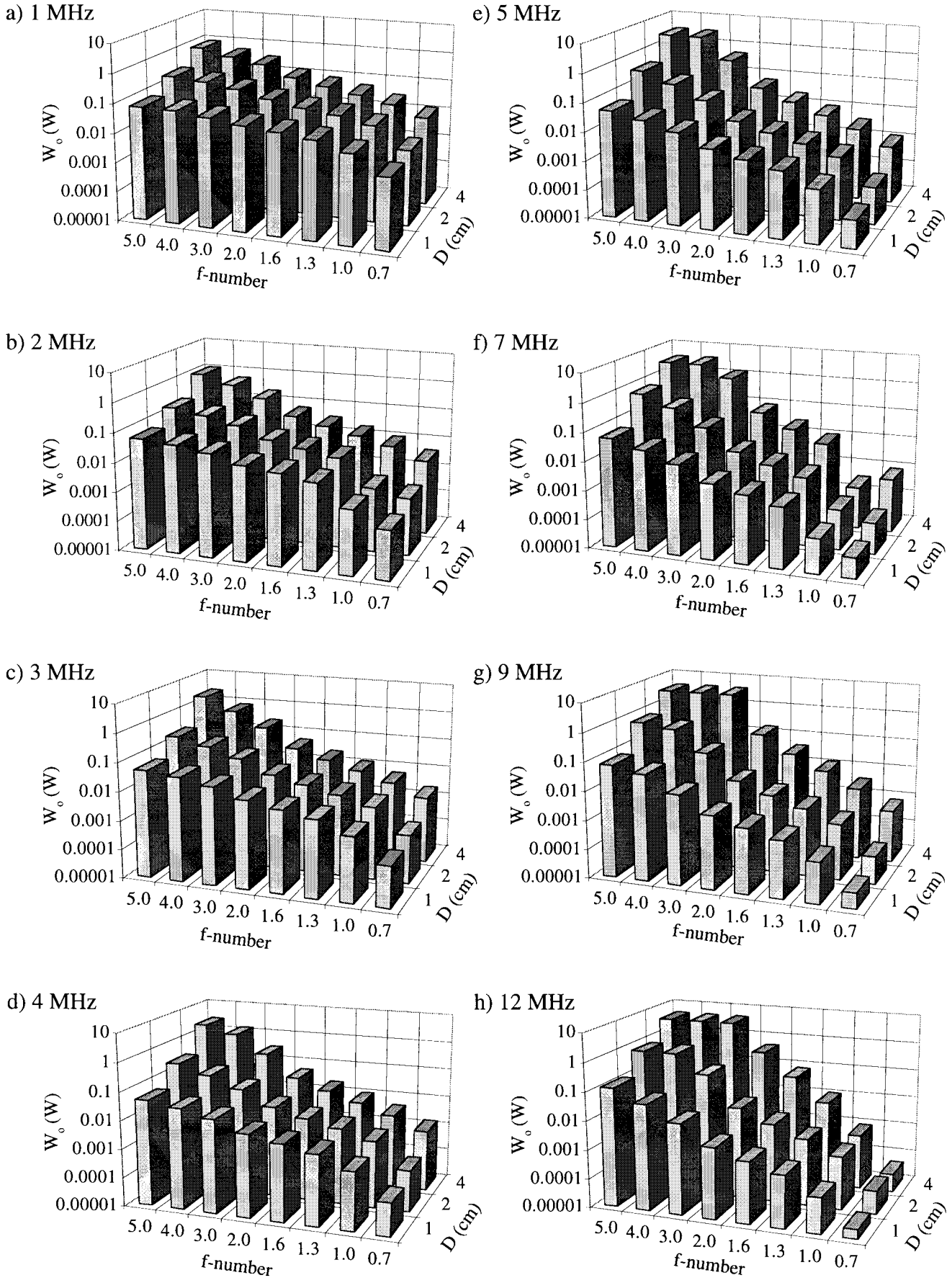

Fig. 4. Source power W_0 as a function of f-number and source diameter D for each of the eight frequencies under the condition that the derated spatial-peak, temporal-average intensity $I_{\mathrm{SPTA.3}}$ is 720 mW/cm^2.

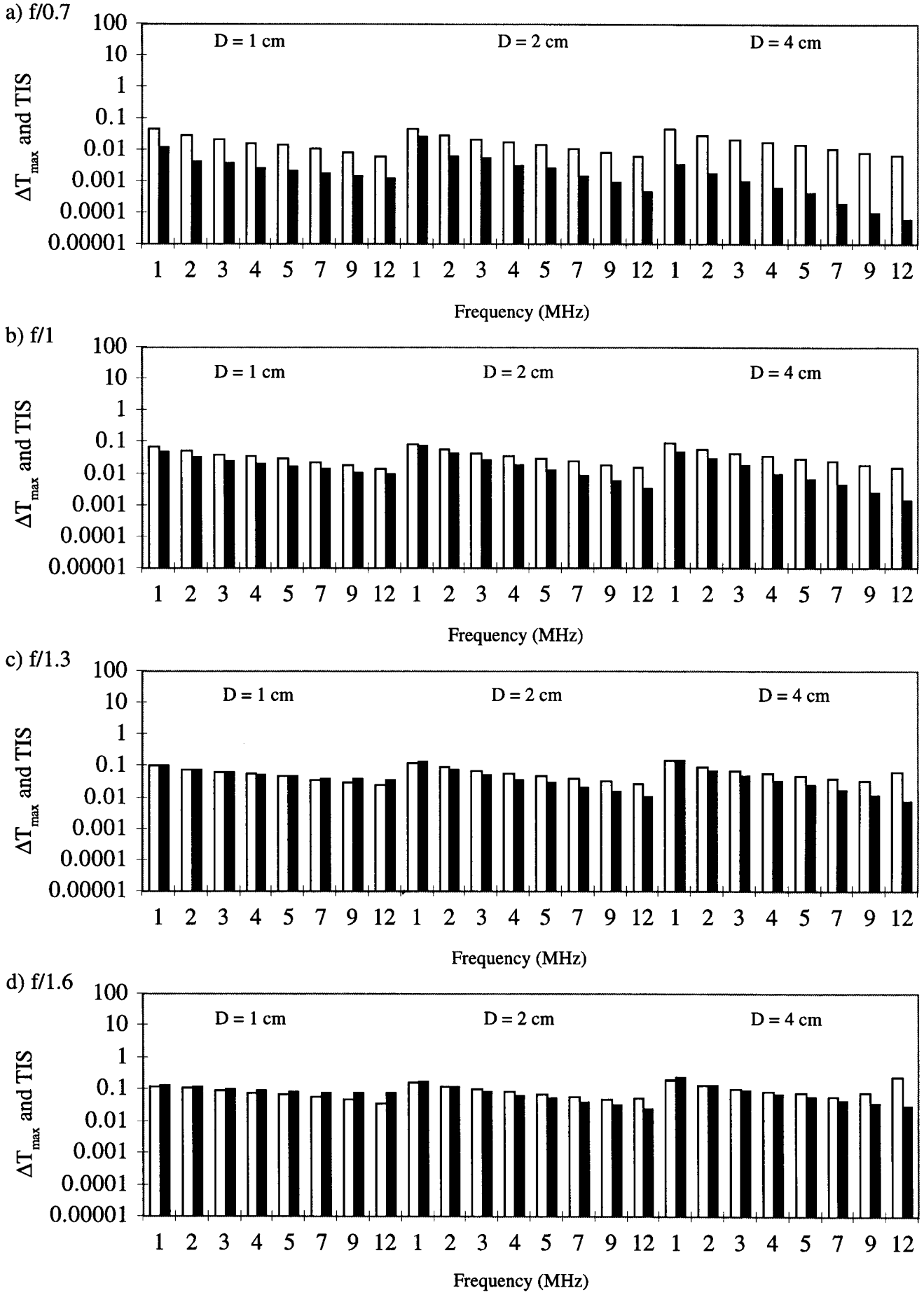
a) f/0.7
b) f/1
c) f/1.3
d) f/1.6
D = 1 cm
D = 2 cm
D = 4 cm
ΔT_max and TIS
100
10
1
0.1
0.01
0.001
0.0001
0.00001
1 2 3 4 5 7 9 12 1 2 3 4 5 7 9 12 1 2 3 4 5 7 9 12
Frequency (MHz)

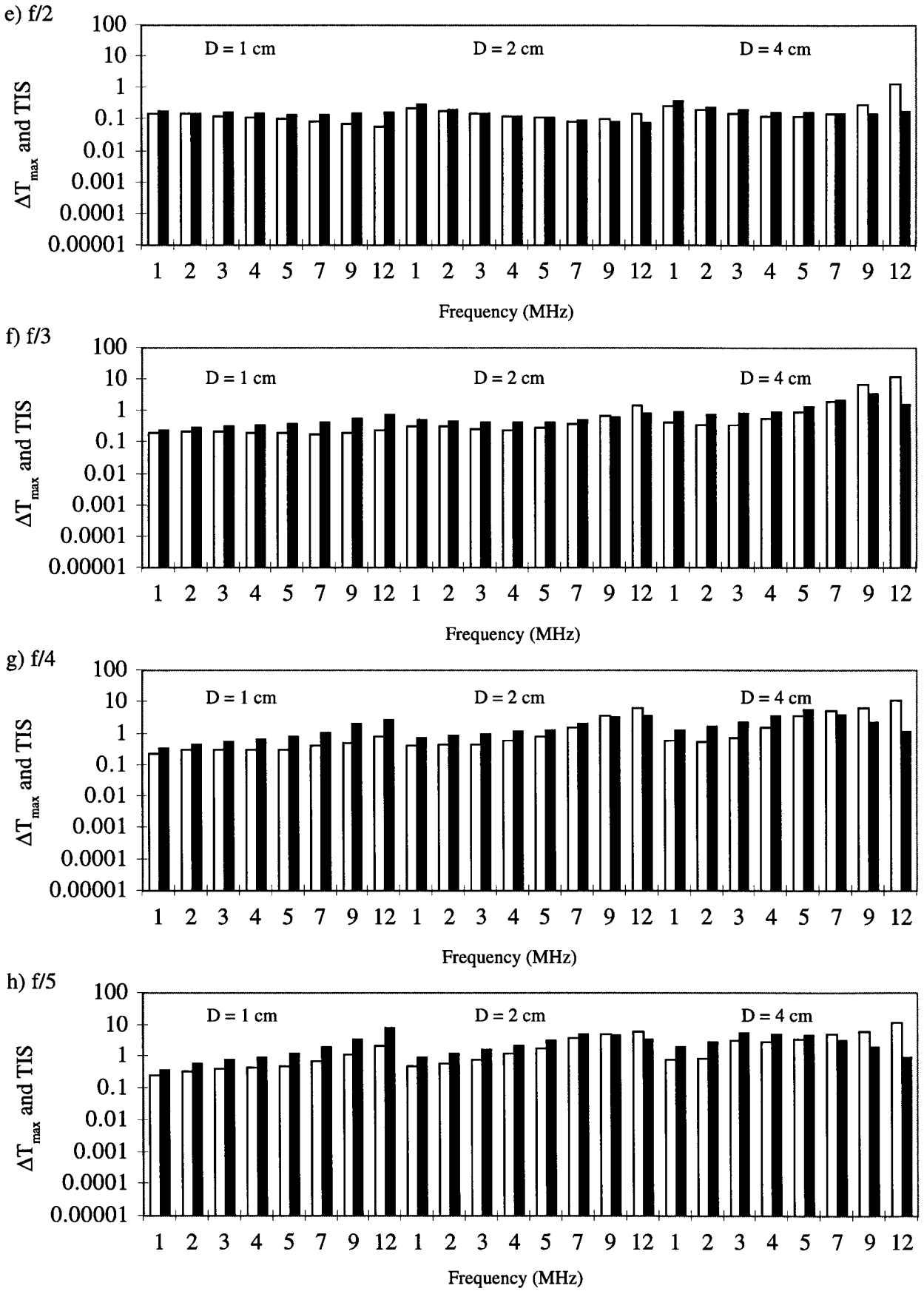

Fig. 5. Paired maximum steady-state temperature increase $\Delta T_{\max}$ (white columns) and unscanned soft-tissue thermal index TIS (black columns) as a function of frequency grouped by f-number under the condition that the derated spatial-peak, temporal-average intensity $I_{\mathrm{SPTA.3}}$ is 720 mW/cm^2. The frequency axis is grouped by the three source diameters.

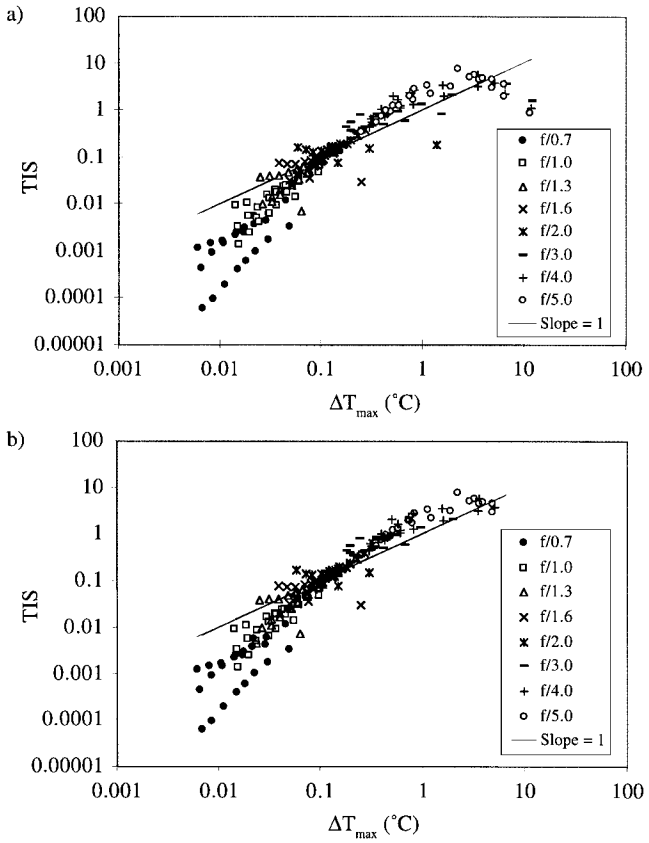

Fig. 6. Unscanned soft-tissue thermal index TIS as a function of maximum steady-state temperature increase $\Delta T_{\max}$ under the condition that the derated spatial-peak, temporal-average intensity $I_{\mathrm{SPTA.3}}$ is 720 mW/cm^2. The straight line denotes TIS = $\Delta T_{\max}$. (a) For all 192 cases. (b) Ten selected $\Delta T_{\max}$-TIS pairs omitted from (a): $f/2.0$ for 12-MHz, 4-cm-diameter; $f/3.0$, $f/4.0$, and $f/5.0$ for 9- and 12-MHz, 4-cm-diameter, and 12-MHz, 2-cm-diameter.

TIS value of these 96 cases is 0.24, which suggests that the TIS would not need to be displayed according to the ODS display requirements [3].

The maximum $\Delta T_{\max}$ value in the $f/2.0$ group is 1.38°C (TIS is 0.18), which occurs for the 12-MHz, 4-cm-diameter case [shown clearly in Fig. 5(e)]. The next highest $\Delta T_{\max}$ value is 0.30°C (TIS is 0.16) for the 9-MHz, 2-cm-diameter case. If the 12-MHz, 4-cm-diameter case is omitted from the $f/2.0$ group, a nonclinical case, then the five lowest f-number groups ($f/0.7$, $f/1.0$, $f/1.3$, $f/1.6$, and $f/2.0$) have a maximum $\Delta T_{\max}$ value that does not exceed 0.30°C, and a maximum TIS value that does not exceed 0.40. This suggests that TIS would not need to be displayed for these 119 $\Delta T_{\max}$-TIS pairs according to the ODS display requirements [3].

The maximum $\Delta T_{\max}$ values in the three highest f-number groups of $f/3.0$, $f/4.0$, and $f/5.0$ are 12.2, 11.7, and 11.5°C. These cases represent a potential for serious concern because their respective displayed TIS values are 1.61, 1.14, and 0.92, which do not inform the system operator of the potentially damaging temperature increases. These three $\Delta T_{\max}$-TIS pairs occur for the 12-MHz, 4-cm-diameter case [Fig. 5(f–h)] which suggests that the

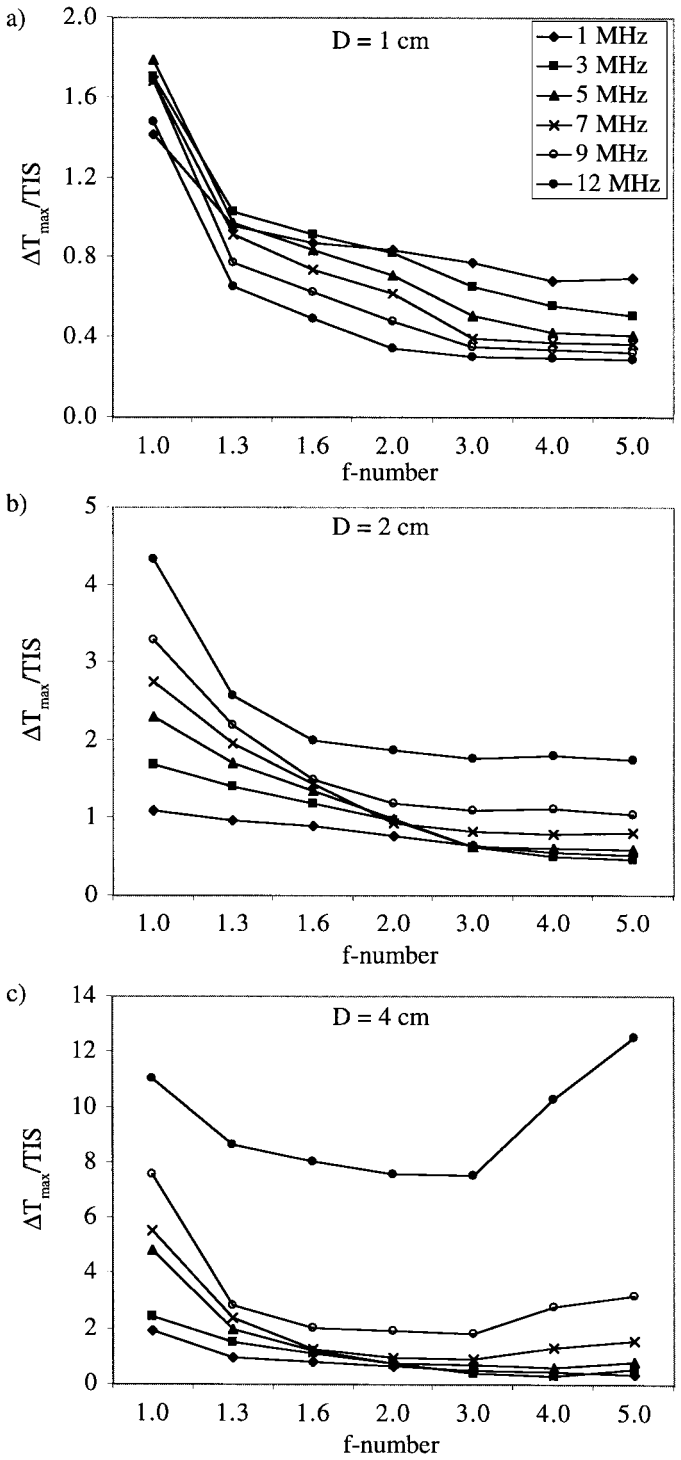

Fig. 7. $\frac{\Delta T_{\max}}{\mathrm{TIS}}$ as a function of f-number under the condition that the derated spatial-peak, temporal-average intensity $I_{\mathrm{SPTA.3}}$ is 720 mW/cm^2. (a) $D = 1$ cm, (b) $D = 2$ cm, and (c) $D = 4$ cm.

TABLE III
MINIMUM AND MAXIMUM VALUES OF $\Delta T_{\max}$, TIS, AND THEIR RATIO GROUPED BY f-NUMBER. EACH f-NUMBER SET INCLUDES 24 CASES.

f-number	$\Delta T_{\max}$(°C)	TIS	$\frac{\Delta T_{\max}}{\text{TIS}}$
0.7	0.006-0.049	0.0001-0.025	1.87-109
1.0	0.014-0.095	0.0014-0.082	1.10-11.0
1.3	0.025-0.15	0.0073-0.15	0.65-8.64
1.6	0.038-0.25	0.026-0.24	0.49-8.04
2.0	0.058-1.38	0.078-0.40	0.35-7.57
3.0	0.18-12.2	0.25-3.60	0.30-7.54
4.0	0.23-11.7	0.33-5.79	0.24-10.3
5.0	0.25-11.5	0.36-7.83	0.29-12.5

longer-focus, higher-frequency, larger-diameter cases that yield high $\Delta T_{\max}$ values are not being properly tracked by the ODSs TIS-calculation procedures. The same lack of proper tracking occurs for many of the shorter-focus cases, as discussed above; but is not a safety concern because $\Delta T_{\max}$ does not exceed 0.3°C. To gain a better understanding of how well $\Delta T_{\max}$ tracks TIS, the ratio quantity $\frac{\Delta T_{\max}}{\text{TIS}}$ is compared as a function of f-number (Fig. 7). For the 12-MHz, 4-cm-diameter cases, $\frac{\Delta T_{\max}}{\text{TIS}}$ values are significantly greater than those of the other 4-cm-diameter cases [Fig. 7(c)]; note that $\Delta T_{\max}$ is significantly greater than TIS for all of the 12-MHz, 4-cm-diameter cases (Fig. 5). Also, TIS underestimates $\Delta T_{\max}$ for all of the 12-MHz, 2-cm-diameter cases [Fig. 7(b)] but not to the extent of the 12-MHz, 4-cm-diameter cases. These longer-focus, $\frac{\Delta T_{\max}}{\text{TIS}} > 1$ cases are shown in the upper right portion of Fig. 6(a) under the slope = 1 curve where the $\Delta T_{\max}$ values are at levels of concern.

Consider the situation in which 10 selected $\Delta T_{\max}$-TIS pairs are omitted from Fig. 6(a), that is, the longer-focus, $\frac{\Delta T_{\max}}{\text{TIS}} > 1$ cases. In addition to the 12-MHz, 4-cm-diameter, $f/2.0$ case discussed above, the following nine longer-focus, larger-diameter, higher-frequency cases are omitted: $f/3.0$, $f/4.0$, and $f/5.0$ for 9- and 12-MHz, 4-cm-diameter and 12-MHz, 2-cm-diameter. The resultant figure [Fig. 6(b)] demonstrates better agreement between $\Delta T_{\max}$ and TIS at the higher $\Delta T_{\max}$ values, that is, TIS generally tracks and slightly overestimates $\Delta T_{\max}$ for the majority of cases. These observations suggest that the ODS procedures may not be applicable for the longer-focus, larger-diameter, higher-frequency sources.

The ODS does not require user information about the location of $\Delta T_{\max}$. To gain this understanding, the axial distance locations of $\Delta T_{\max}$ (denoted as $d_{\Delta T_{\max}}$) are shown in Fig. 8 in terms of the normalized distance $\frac{d_{\Delta T_{\max}}}{\text{ROC}}$ as a function of f-number and source diameter for each of the eight frequencies. For all 192 cases, $d_{\Delta T_{\max}} < \text{ROC}$, the geometric focus location. For the lower f-number cases, $d_{\Delta T_{\max}}$ is approximately near the geometric focus. As the frequency increases for these lower f-number cases, $d_{\Delta T_{\max}}$ moves closer to the geometric focus. However, for the higher f-number cases in each frequency set for $f \geq 3$ MHz, $d_{\Delta T_{\max}}$ appears to behave anomalously wherein $d_{\Delta T_{\max}}$ abruptly jumps to near the transducer surface. This anomalous behavior becomes more prevalent at higher frequencies and larger source diameters.

This anomalous behavior also is demonstrated, but to a lesser extent, for $I_{\text{SPTA.3}}$ locations where the axial distance locations of $I_{\text{SPTA.3}}$ (denoted as $d_{\text{ISPTA.3}}$) are shown in terms of the normalized distance $\frac{d_{\text{ISPTA.3}}}{\text{ROC}}$ as a function of f-number and source diameter for each of the eight frequencies (Fig. 9). For all 192 cases, $d_{\text{ISPTA.3}} < \text{ROC}$, and has the same general trends as for $d_{\Delta T_{\max}}$. However, the $d_{\text{ISPTA.3}}$ anomalous behavior does not occur until 4 MHz, and does not appear to affect as many cases at the higher frequencies.

To gain an understanding of this anomalous behavior, axial distributions of the steady-state temperature increase $\Delta T_{ss}(z)$ and the derated temporal-average intensity $I_{\text{TA.3}}(z)$ for the 2-MHz and 7-MHz cases are evaluated. The anomalous behavior for $d_{\Delta T_{\max}}$ and $d_{\text{ISPTA.3}}$ does not occur for the 2-MHz cases, but occurs for the 7-MHz cases. Fig. 10 shows $\Delta T_{ss}(z)$ for the 2- and 7-MHz cases. The 7-MHz cases [Fig. 10(d–f)] demonstrate clearly the behavior of the $\Delta T_{\max}$ location. For the lower f-number cases, $d_{\Delta T_{\max}}$ is dominated by the peak near the focal region for which the distance to the geometric focus is not very long and thus not strongly dominated by the derating (attenuation) factor. However, for the higher f-number cases, where the distance to the geometric focus is greater, the $\Delta T_{ss}(z)$ peak near the geometric focus is observable, although its magnitude is less than that of $\Delta T_{\max}$. Thus, the attenuation has a greater affect on $\Delta T_{ss}(z)$ for the longer path lengths. The maximum $\Delta T_{ss}(z)$ value, the $\Delta T_{\max}$ value, can be thought of as "skipping" from the peak near the focal region to near the transducer surface as the f-number, and thus the attenuation to the focal region, both increase. The 2-MHz cases [Fig. 10(a–c)] do not exhibit this anomalous behavior because the attenuation is less, and thus does not have a dominating effect on the axial distributions of $\Delta T_{ss}(z)$.

Fig. 11 shows the derated temporal-average intensity axial profile $I_{\text{TA.3}}(z)$ for the 2- and 7-MHz cases. Note that for the 7-MHz, 1-cm-diameter cases [Fig. 11(d)], the absolute $I_{\text{TA.3}}(z)$ peak locations, $d_{\text{ISPTA.3}}$, occur at or near their respective focal regions. However, for the larger-diameter cases [Fig. 11(e–f)], $d_{\text{ISPTA.3}}$ occurs either at or near their respective focal regions, or at the transducer surface. For these larger-diameter cases where $d_{\text{ISPTA.3}}$ occurs at the transducer surface, the local $I_{\text{TA.3}}(z)$ peaks are observed near the focal regions, but the magnitudes of these peaks are less than the absolute $I_{\text{TA.3}}(z)$ peaks. These are observed for 2 cm, $f/5$ [Fig. 11(e)] and for 4 cm, $f/4$ and $f/5$ [Fig. 11(f)], and result in the anomalous behavior observed in Fig. 9(f). The cause of this is principally due to the combination of the greater attenuation at the higher frequencies and the relatively long ROC (distance to the focal region). The 2-MHz cases [Fig. 11(a–c)] do not exhibit this anomalous behavior because the attenuation is less and thus does not have a dominating effect on the axial distributions of $\Delta T_{ss}(z)$.

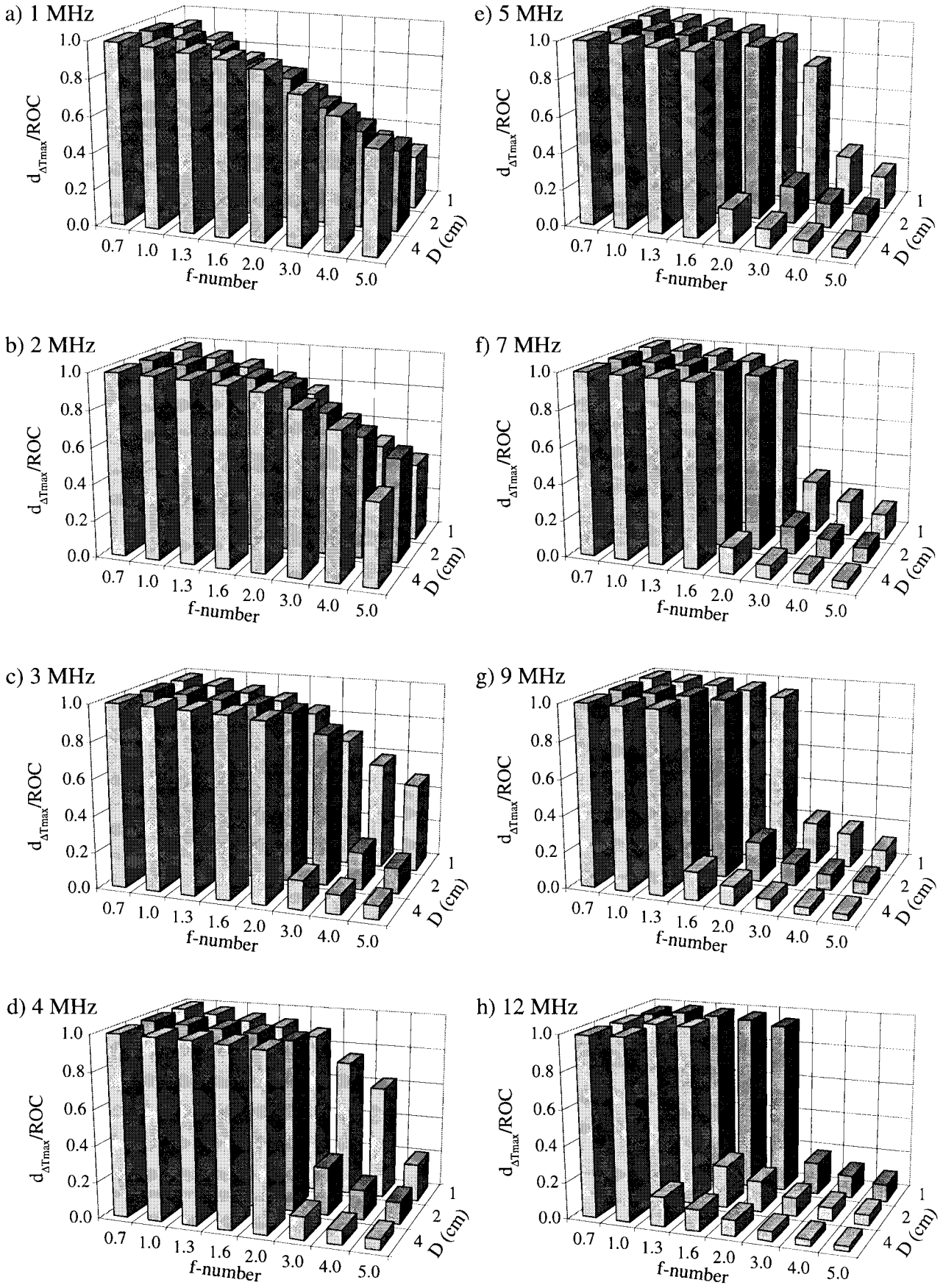

Fig. 8. Normalized location of the maximum steady-state temperature increase $\frac{d_{\Delta T_{\max}}}{\mathrm{ROC}}$ as a function of f-number and source diameter D under the condition that the derated spatial-peak, temporal-average intensity $I_{\mathrm{SPTA.3}}$ is 720 mW/cm^2. $d_{\Delta T_{\max}}$ is the axial distance location of $\Delta T_{\max}$.

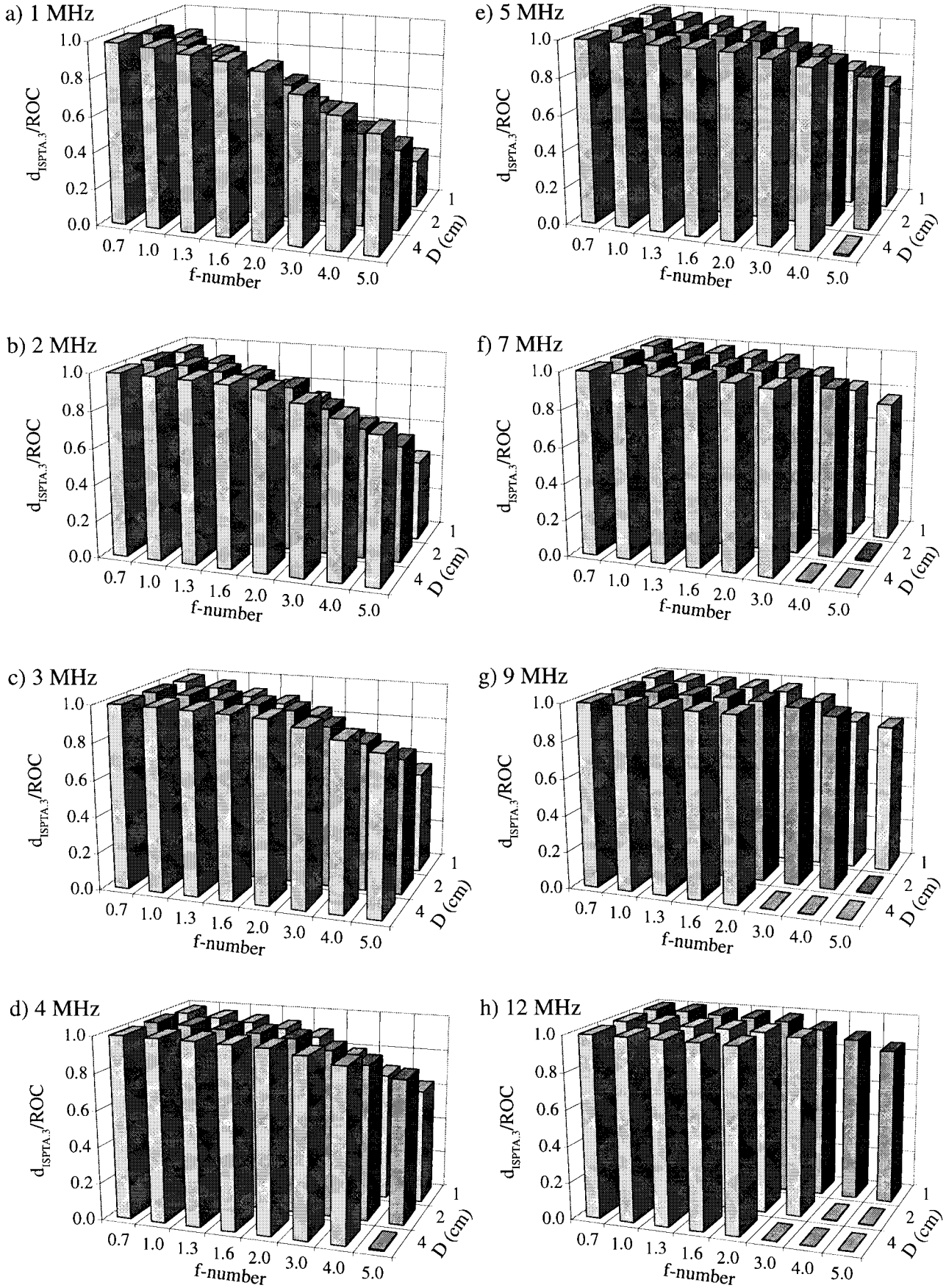

Fig. 9. Normalized location of the derated spatial-peak temporal-average intensity $\frac{d_{\mathrm{ISPTA.3}}}{\mathrm{ROC}}$ as a function of f-number and source diameter D under the condition that the derated spatial-peak, temporal-average intensity $I_{\mathrm{SPTA.3}}$ is 720 mW/cm^2. $d_{\mathrm{ISPTA.3}}$ is the axial distance location of $I_{\mathrm{SPTA.3}}$.

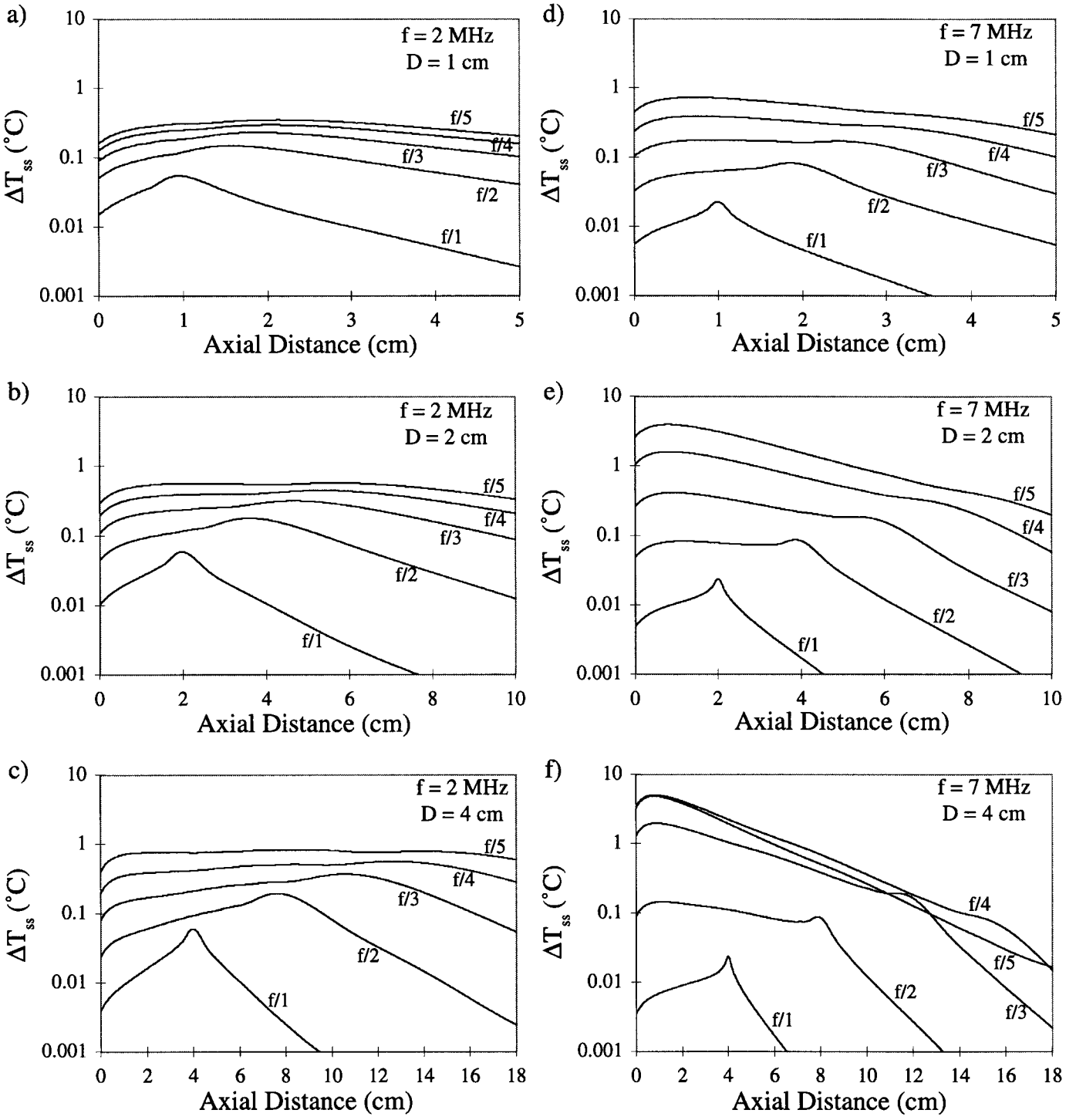

Fig. 10. Steady-state temperature increase $\Delta T_{ss}(z)$ as a function of axial distance for 2 and 7 MHz under the condition that the derated spatial-peak, temporal-average intensity $I_{\mathrm{SPTA.3}}$ is 720 mW/cm^2. Each panel shows $I_{\mathrm{TA.3}}(z)$ as a function of f-number.

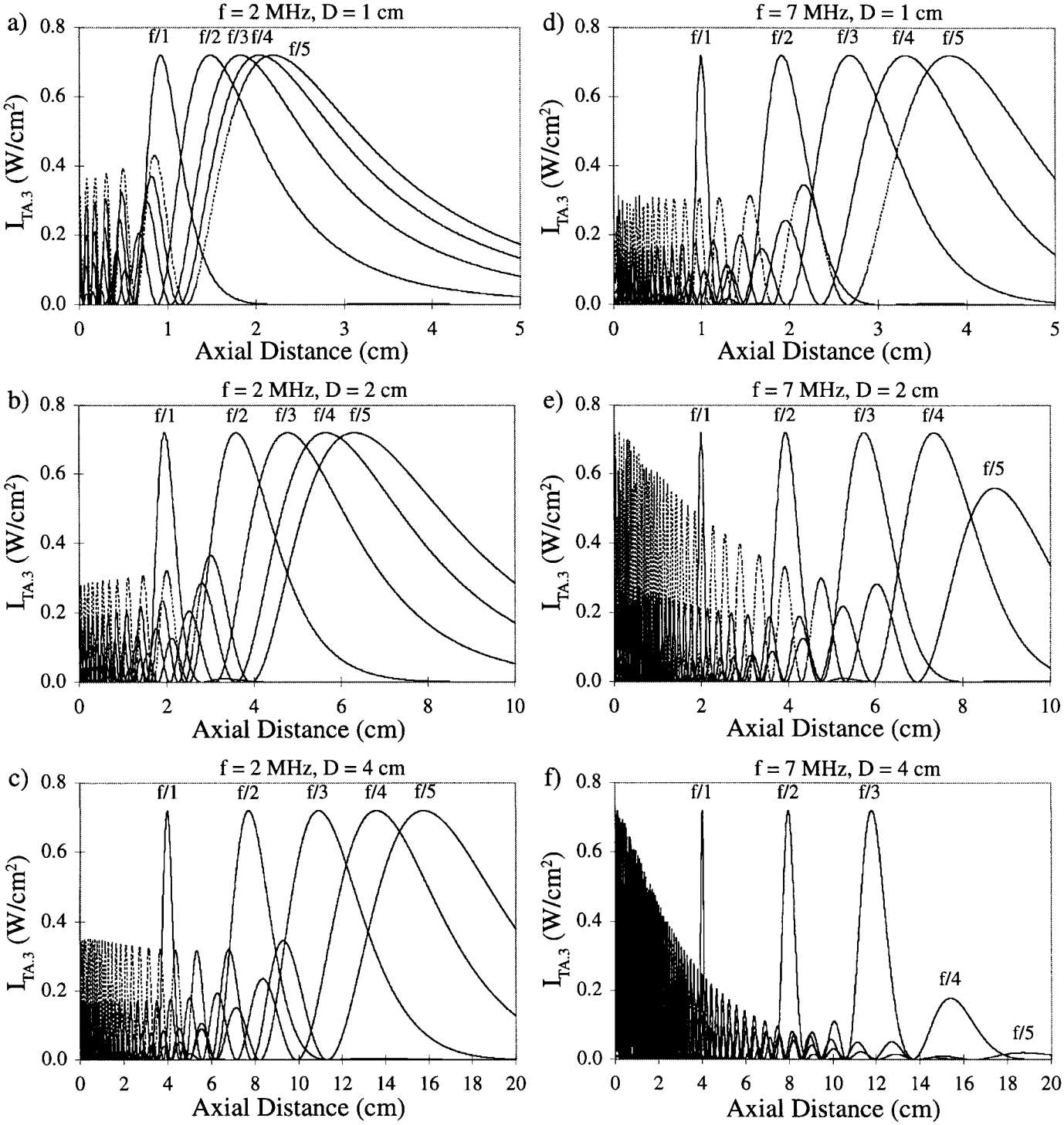

Fig. 11. Derated temporal-average intensity $I_{\mathrm{TA.3}}(z)$ as a function of axial distance for 2 and 7 MHz under the condition that the derated spatial-peak, temporal-average intensity $I_{\mathrm{SPTA.3}}$ is 720 mW/cm^2. Each panel shows $I_{\mathrm{TA.3}}(z)$ as a function of f-number.

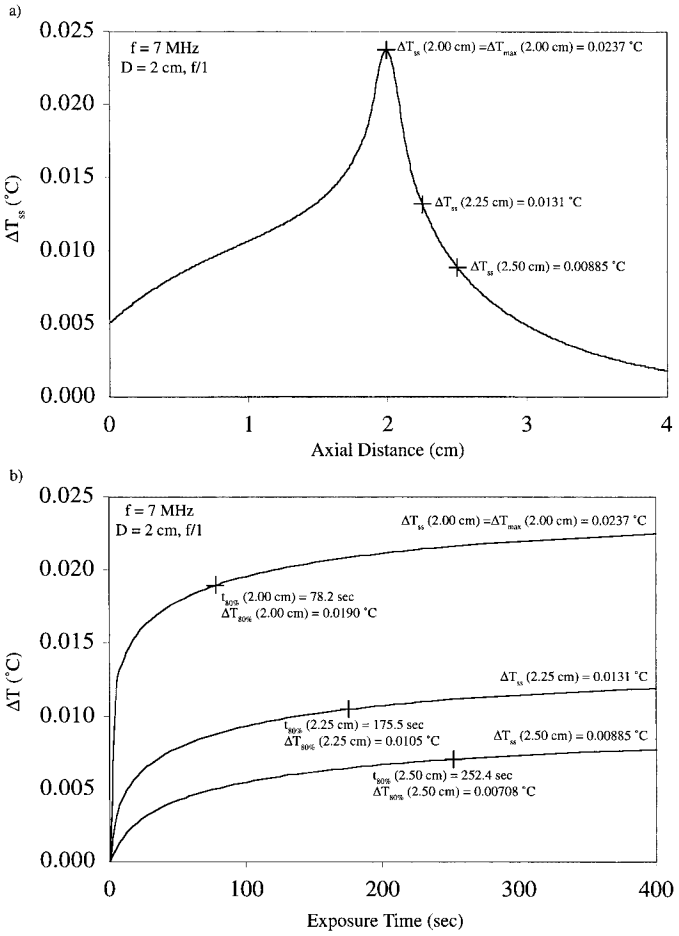

Fig. 12. (a) Steady-state temperature increase $\Delta T_{ss}(z)$ as a function of axial distance for the 7-MHz, 2-cm-diameter, $f/1$ case under the condition that the derated spatial-peak, temporal-average intensity $I_{\mathrm{SPTA.3}}$ is 720 mW/cm^2. The three crosses on the $\Delta T_{ss}(z)$ profile, one at $\Delta T_{\max}$, denote the axial distances at which the transient temperature increases are evaluated. (b) Transient temperature increase $\Delta T(t)$ as a function of exposure time for the three axial locations marked in (a) for which both $t_{80\%}$ and $\Delta T_{80\%}$ are denoted by the crosses. $t_{80\%}$ is the time at which the temperature increase $\Delta T_{80\%}$ reaches 80% of its steady-state value at that axial distance.

The estimation of TIS is based on the maximum value of the steady-state temperature increases under the condition in which the beam remains stationary [3]. Although not included within the ODSs TIS calculation, the time rate of change of temperature is an important exposure quantity. The axial distribution of the steady-state temperature increase $\Delta T_{ss}(z)$ is shown in Fig. 12(a) for the 7-MHz, 2-cm-diameter, $f/1$ case. Three crosses are denoted at three different axial distances at which three different steady-state temperature increases are noted. Temperature increases as a function of exposure time for the three denoted axial distances are shown in Fig. 12(b). One of the crosses [Fig. 12(a)] is located at the axial distance of maximum $\Delta T_{ss}(z)$, which is at $z = 2.00$ cm and $d_{\Delta T_{\max}}$. The upper curve in Fig. 12(b) shows the temporal dependency of temperature increase that is quantified in terms of time ($t_{80\%}$) at which the temperature increase ($\Delta T_{80\%}$) reaches 80% of its steady-state value at that axial distance. At $d_{\Delta T_{\max}}$, $t_{80\%} = 78.2$ sec and $\Delta T_{80\%} = 0.0190$°C. However, at the other two axial locations, the temporal dependencies of temperature increase are different.

A more complete evaluation of the temporal dependency of temperature increase was conducted for all three source diameters (1, 2, and 4 cm) at two frequencies (2 and 7 MHz) for five f-numbers ($f/1$, $f/2$, $f/3$, $f/4$, and $f/5$) (Fig. 13). Each $t_{80\%}$ profile follows the same general pattern as a function of axial distance. For each of the 7-MHz cases, the axial distances of the minimum $t_{80\%}$ values are, in general, near the respective focal regions. However, for the 2-MHz cases, the axial distances of the minimum $t_{80\%}$ values tend not to be near the respective focal regions but rather closer to the transducer. Also, the minimum $t_{80\%}$ values increase as a function of increasing f-number, and decrease as a function of increasing frequency. The global minimum $t_{80\%}$ values are 97.2 and 59.7 sec for the 15 2-MHz and 15 7-MHz cases, respectively, both of which are for the 1-cm-diameter, $f/1$ cases.

The axial distances at which the minimum $t_{80\%}$ values occur for each of the cases evaluated (Fig. 13) are either at the focal region or between the source and focal region. Fig. 14(a) compares the axial distances of the minimum $t_{80\%}$ values to the axial distances of $d_{\mathrm{ISPTA.3}}$, $d_{\Delta T_{\max}}$, and minimum beamwidth for each of the 30 2-and 7-MHz cases examined in Fig. 13. The axial distances for these four quantities are essentially the same under $f/1$ conditions. However, as the f-number increases, there is a clear separation of axial distances at which these quantities occur. This is markedly shown for the cases that behave in an anomalous manner, particularly for the 7-MHz, 4-cm-diameter cases. Even for the anomalous cases, as with all other cases, the minimum beamwidth location is consistently closest to that of the minimum $t_{80\%}$ values. Excluding the anomalous cases, the next closest to the minimum $t_{80\%}$ values is $d_{\mathrm{ISPTA.3}}$, and the furthest is $d_{\Delta T_{\max}}$.

Fig. 14(b) compares the time to reach 80% of the maximum (steady-state) temperature increase for each of four quantities at their respective axial distances: $\Delta T_{\max}$, $I_{\mathrm{SPTA.3}}$, minimum beamwidth, and minimum $t_{80\%}$. The minimum $t_{80\%}$ time is the shortest time required for the temperature increase to reach 80% of the maximum temperature increase (the minimums in Fig. 13). The $t_{80\%}$ values for these four quantities are essentially the same under $f/1$ conditions. However, as the f-number increases, there is a clear separation of $t_{80\%}$ values for these quantities. This is markedly shown for the cases that behave in an anomalous manner, particularly for the 7-MHz, 2- and 4-cm-diameter cases. Even for these anomalous cases, as with all other cases, the $t_{80\%}$ values of the minimum beamwidth are consistently closest to those of the minimum $t_{80\%}$. Also, note that the $t_{80\%}$ values at the axial distances for $\Delta T_{\max}$ are on the order of one to three minutes, and in some cases are often much greater.

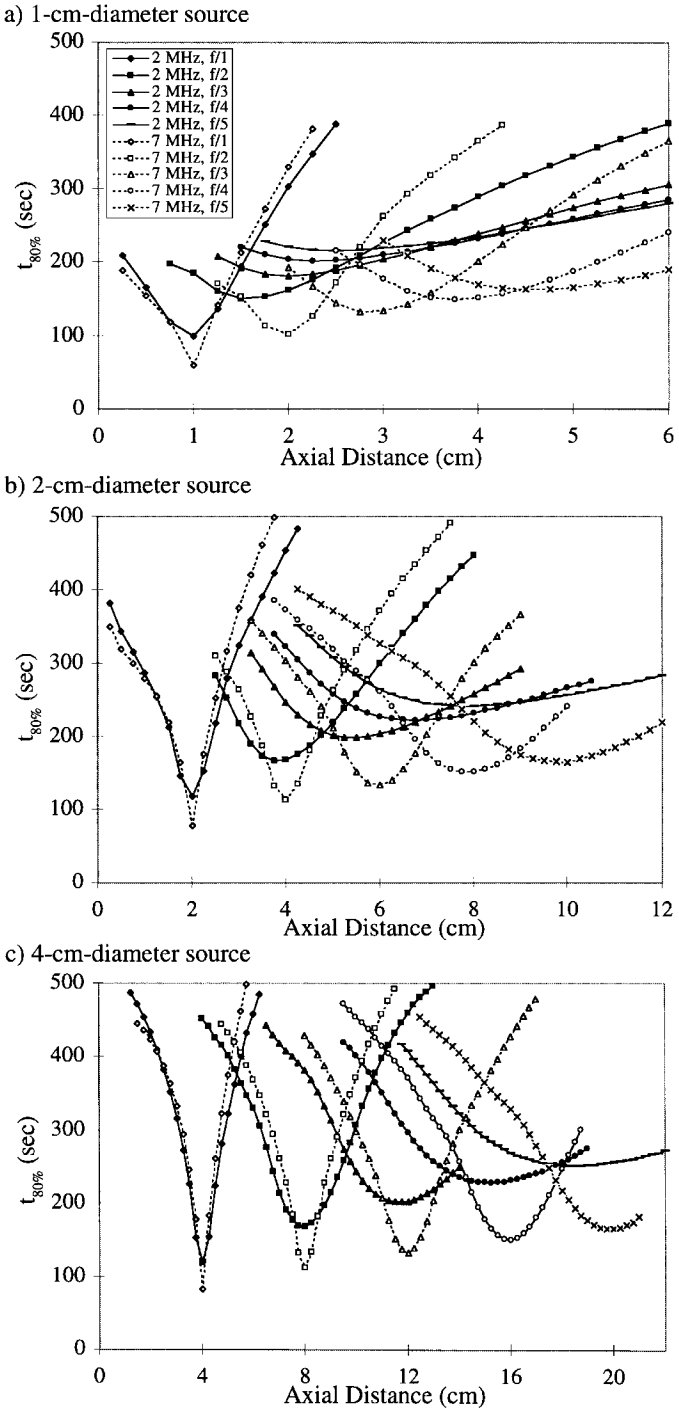

Fig. 13. $t_{80\%}$ profiles as a function of axial distance for the 2- and 7-MHz cases under the condition that the derated spatial-peak, temporal-average intensity $I_{\mathrm{SPTA.3}}$ is 720 mW/cm^2.

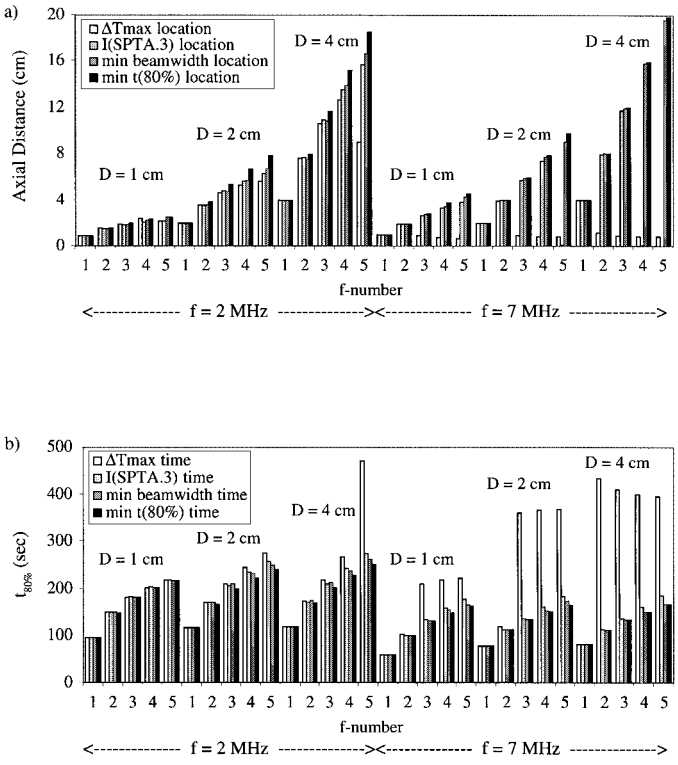

Fig. 14. (a) Axial distance as a function of f-number for the 2- and 7-MHz cases where the minimum $t_{80\%}$ values occur for $\Delta T_{\max}$, $I_{\mathrm{SPTA.3}}$, minimum beamwidth and minimum $t_{80\%}$. (b) $t_{80\%}$ as a function of f-number for the 2- and 7-MHz cases for $\Delta T_{\max}$, $I_{\mathrm{SPTA.3}}$, minimum beamwidth and minimum $t_{80\%}$ at their respective axial distances. For both graphs, the f-number axis is grouped by frequency and subgrouped by source diameter. All cases are under the condition that the derated spatial-peak, temporal-average intensity $I_{\mathrm{SPTA.3}}$ is 720 mW/cm^2.

IV. Summary

The ODSs unscanned soft-tissue thermal index TIS generally underestimates $\Delta T_{\max}$ for f-numbers ≤ 2. For these lower f-number cases, and because of the FDAs $I_{\mathrm{SPTA.3}}$ limit of 720 mW/cm^2, $\Delta T_{\max} \leq 0.30$°C and TIS ≤ 0.40. This suggests that TIS would not need to be displayed according to the ODS display requirements. However, for the longer-focus cases ($f/3$, $f/4$, and $f/5$), TIS generally tracks or slightly overestimates $\Delta T_{\max}$. Also, for these longer-focus, higher-frequency cases evaluated, the procedure for calculating TIS appears to break down. Even though the ODS does not address either the location of $\Delta T_{\max}$ or the temporal dependency of temperature increase, both were evaluated. For the shorter-focus cases, the location of $\Delta T_{\max}$ is near to the geometric focus. However, as the f-number increases for each frequency, the location of $\Delta T_{\max}$ moves toward the source. For the longer-focus cases, and for $f \geq 3$ MHz, the location of $\Delta T_{\max}$ is very close to the source. Thus, the system operator has no way to even estimate the axial distance where the steady-state temperature increase is a maximum. Also, in order for the ultrasound beam to achieve 80% of the steady-state $\Delta T_{\max}$ value, at least 1 minute is required for the beam to

remain stationary during an exam. This suggests that the TIS procedure is very conservative at estimating temperature increase.

References

[1] *501(k) Guide for Measuring and Reporting Acoustic Output of Diagnostic Ultrasound Medical Devices*. Rockville, MD: Center for Devices and Radiological Health, US Food and Drug Administration, 1985.

[2] *Diagnostic Ultrasound Guidance Update*. Rockville, MD: Center for Devices and Radiological Health, US Food and Drug Administration, 1987.

[3] *Standard for Real-Time Display of Thermal and Mechanical Indices on Diagnostic Ultrasound Equipment*. Laurel, MD: AIUM Publications, 1992.

[4] *Revised 510(k) Diagnostic Ultrasound Guidance for 1993*. Rockville, MD: Center for Devices and Radiological Health, US Food and Drug Administration, 1993.

[5] *Use of Mechanical Index in Place of Spatial Peak, Pulse Average Intensity in Determining Substantial Equivalence*. Rockville, MD: Center for Devices and Radiological Health, US Food and Drug Administration, 1994.

[6] *Information for Manufacturers Seeking Marketing Clearance of Diagnostic Ultrasound Systems and Transducers*. Rockville, MD: Center for Devices and Radiological Health, US Food and Drug Administration, 1997.

[7] *Implementation of the Principle of As Low As Reasonably Achievable (ALARA) for Medical and Dental Personnel*. National Council on Radiation Protection and Measurements (NCRP), Report No. 107, Bethesda, MD, 1990.

[8] D. S. Ellis and W. D. O'Brien, Jr., "The monopole-source solution for estimating tissue temperature increases for focused diagnostic ultrasound," *IEEE Trans. Ultrason., Ferroelect., Freq. Contr.*, vol. 43, pp. 88–97, 1996.

[9] W. L. Nyborg, "Solutions to the bio-heat transfer equation," *Phys. Med. Biol.*, vol. 33, pp. 785–792, 1988.

[10] *Exposure Criteria for Medical Diagnostic Ultrasound: I. Criteria Based on Thermal Mechanisms*. National Council on Radiation Protection and Measurements (NCRP), Report No. 113, Bethesda, MD, 1992.

[11] *Bioeffects and Safety of Diagnostic Ultrasound*. Laurel, MD: AIUM Publications, 1993.

William D. O'Brien, Jr. (S'64–M'70–SM'79–F'89) received the B.S., M.S., and Ph.D. degrees in 1966, 1968, and 1970, from the University of Illinois, Urbana-Champaign.

From 1971 to 1975 he worked with the Bureau of Radiological Health (currently the Center for Devices and Radiological Health) of the U.S. Food and Drug Administration. Since 1975, he has been at the University of Illinois, where he is a Professor of Electrical and Computer Engineering and of Bioengineering, College of Engineering; Professor of Bioengineering, College of Medicine; Professor of Nutritional Sciences, College of Agricultural, Consumer and Environmental Sciences; a Research Professor in the Beckman Institute for Advanced Science and Technology; and a Research Professor in the Coordinated Science Laboratory. He is the Director of the Bioacoustics Research Laboratory and is the Program Director of the NIH Radiation Biophysics and Bioengineering in Oncology Training Program. His research interests involve the many areas of ultrasound-tissue interaction, including spectroscopy, risk assessment, biological effects, tissue characterization, dosimetry, blood-flow measurements, acoustic microscopy and imaging, for which he has published 210 papers.

Dr. O'Brien is Editor-in-Chief of the *IEEE Transactions on Ultrasonics, Ferroelectrics, and Frequency Control*. He is a Fellow of the Institute of Electrical and Electronics Engineers (IEEE), the Acoustical Society of America (ASA), and the American Institute of Ultrasound in Medicine (AIUM). He is a Founding Fellow of the American Institute of Medical and Biological Engineering. Dr. O'Brien was recipient of the IEEE Centennial Medal (1984), the AIUM Presidential Recognition Awards (1985 and 1992), the AIUM/WFUMB Pioneer Award (1988), the IEEE Outstanding Student Branch Counselor Award for Region 4 (1989), the AIUM Joseph H. Holmes Basic Science Pioneer Award (1993), and the IEEE Ultrasonics, Ferroelectrics, and Frequency Control Society Distinguished Lecturer (1997-1998). He received the IEEE Ultrasonics, Ferroelectrics, and Frequency Control Society's Achievement Award for 1998.

He has served as Co-Chair of the 1981 IEEE Ultrasonic Symposium, and General Chair of the 1988 IEEE Ultrasonics Symposium, and is Co-Chair of both the 2001 and 2003 IEEE Ultrasonics Symposia. He was Secretary-Treasurer (1972-1980), Vice President (1981), and President (1982-1983) of the IEEE Sonics and Ultrasonics Group (currently the IEEE Ultrasonics, Ferroelectrics, and Frequency Control Society). He was Treasurer (1982-1985), President-Elect (1986-1988) and President (1988-1991) of the American Institute of Ultrasound in Medicine. He has served on the Board of Directors (1988-1993) of the American Registry of Diagnostic Medical Sonographers, and he was Treasurer (1991-1994) of the World Federation for Ultrasound in Medicine and Biology.